A Conceptual View on Inertial Oscillations and Nocturnal Low-Level Jets

B. J. H. VAN DE WIEL

Meteorology and Air Quality, Wageningen University and Research Centre, Wageningen, and Turbulence and Vortex Dynamics, Department of Applied Physics, Eindhoven Technical University, Eindhoven, Netherlands

A. F. MOENE AND G. J. STEENEVELD

Meteorology and Air Quality, Wageningen University and Research Centre, Wageningen, Netherlands

P. BAAS AND F. C. BOSVELD

Royal Netherlands Meteorological Institute, De Bilt, Netherlands

A. A. M. HOLTSLAG

Meteorology and Air Quality, Wageningen University and Research Centre, Wageningen, Netherlands

ABSTRACT

In the present work Blackadar's concept of nocturnal inertial oscillations is extended. Blackadar's concept describes frictionless inertial oscillations above the nocturnal inversion layer. The current work includes frictional effects within the nocturnal boundary layer. It is shown that the nocturnal wind speed profile describes an oscillation around the nocturnal equilibrium wind vector, rather than around the geostrophic wind vector (as in the Blackadar case). By using this perspective, continuous time-dependent wind profiles are predicted. As such, information on both the height and the magnitude of the nocturnal low-level jet is available as a function of time. Preliminary analysis shows that the proposed extension performs well in comparison with observations when a simple Ekman model is used to represent the equilibrium state in combination with a realistic initial velocity profile.

In addition to jet dynamics, backward inertial oscillations are predicted at lower levels close to the surface, which also appear to be present in observations. The backward oscillation forms an important mechanism behind weakening low-level winds during the afternoon transition. Both observational and theoretical modeling studies are needed to explore this phenomenon further.

1. Introduction

More than 50 years ago, Blackadar (1957; hereafter B57) introduced his conceptual model for nocturnal inertial oscillations. Since then, it has been generally known that inertial oscillations (IOs) form an important mechanism behind the occurrence of low-level wind maxima or low-level jets (LLJs)—for example, in Australia and over the European plains (Thorpe and Guymer 1977; Van Ulden and Wieringa 1996; Baas et al. 2009). Low-level jets are not solely initiated by IOs: studies over the American Great Plains (e.g., Whiteman et al. 1997; Banta et al. 2002; Lundquist 2003) revealed that other mechanisms such as frontal dynamics may dominate over IOs in those areas (see also Ostdiek and Blumen 1997). In this study we will confine ourselves to low-level jets related to inertial oscillations solely. Although IOs may be modulated by slope effects (Shapiro and Fedorovich 2009), here we will restrict our analysis to flat terrain.

The importance of LLJs for nocturnal boundary layer (NBL) studies is obvious since they appear to be a source of shear-driven turbulence: "shear generation of turbulence at the top of the surface inversion layer may be primarily due to formation of a low-level nocturnal jet where turbulence is enhanced by shear on the underside of the jet . . . " (Mahrt 1998, p. 273). Particularly, studies

Corresponding author address: B. J. H. van de Wiel, Turbulence and Vortex Dynamics, Department of Applied Physics, Eindhoven Technical University, Postbus 513, Eindhoven, 5600 MB, Netherlands.
E-mail: b.j.h.v.d.wiel@tue.nl

by Banta et al. (2003, 2006) and Banta (2008) succeeded in relating jet-based properties, such as jet-nose height and speed, to major mixing characteristics of the NBL. In a more applied sense, LLJs have numerous implications (Baas et al. 2009) in fields like aviation (Wittich et al. 1986), air pollution (McNider et al. 1988; Weil et al. 2006; Beyrich 1994), and bird migration studies (Liechti and Schaller 1999). LLJs are also important in the field of renewable energy (e.g., for accurate prediction of wind energy yields; Storm et al. 2009).

Owing to its simple and elegant structure, the B57 concept has become standard in educational textbooks on boundary layer (BL) meteorology. According to B57, nocturnal winds above the inversion layer perform an undamped oscillation around the geostrophic wind with a period of $2\pi/f$ (where f is the Coriolis parameter) and an amplitude equal to the magnitude of the ageostrophic velocity component at sunset. Obviously, B57 theory is not applicable within the NBL: the ageostrophic component of the wind is largest near the ground. Naive extrapolation of B57 would imply maximum IO at the ground level, which clearly conflicts with the observation that wind speeds remain zero at the surface.

Therefore, an important extension to B57 within the NBL was proposed by Thorpe and Guymer (1977). They introduced a bulk approach to model the diurnal wind cycle. For the nocturnal case, the model consists of a frictionless upper layer (above the NBL) and a lower layer (within the NBL). In the latter, frictional effects are parameterized by an empirical drag law. The model predicts the supergeostrophic behavior at higher levels after sunset and suggests decreasing winds near the surface. However, due to the bulk nature of the model, the predicted winds depart from real wind observations, as no continuous wind profiles are predicted.

In fact, continuous velocity profiles are obtained by full analytical studies, such as Singh et al. (1993) and Tan and Farahani (1998) and, recently, Shapiro and Fedorovich (2010). Although these studies clearly improve our understanding of diurnal dynamics of the wind profile, their approach is usually rather complex. Moreover, almost all analytical studies adopt an approach in which the eddy diffusivity varies in time, but without any (or realistic) dependence of the eddy diffusivity on height and stability [although some height dependence has been included by Tan and Farahani (1998)]. Clearly, such dependence is preferred in order to predict realistic wind dynamics close to the ground.

The present study aims at combining some of the beneficial features of the above approaches, namely by introducing a height-continuous model with the same simplicity as the Blackadar model but with a formulation of frictional effects in the boundary layer. As a consequence, it will appear that the *nocturnal velocity profile* does not describe an *inertial oscillation around the geostrophic wind vector*, but rather shows an *oscillation around the equilibrium wind vector* (this makes B57 a special case, for a frictionless equilibrium). As initial deviation from equilibrium depends on height, continuous and time-dependent wind profiles are obtained that show typical nocturnal LLJ characteristics. The new model may have both educational and practical value, as it provides information on the timing, magnitude, and height of the LLJ. This will be illustrated by comparison with an observational case.

Although the concept was initially intended to explain LLJ behavior, it yielded an interesting additional feature: besides supergeostrophic winds at higher levels (forward inertial oscillation), the model predicts a distinct "backward inertial oscillation" at lower levels. It will be shown that this backward inertial oscillation may explain the fact that near-surface winds tend to weaken as the evening sets in. Finally, implications of the findings will be discussed.

2. The Blackadar model

The B57 model uses the well-known boundary layer equations for the mean wind components U and V (we omit the overbar for mean variables; e.g., Stull 1988):

$$\frac{\partial U}{\partial t} = fV + \frac{\partial \tau_x/\rho}{\partial z} \qquad (1)$$

and

$$\frac{\partial V}{\partial t} = f(G - U) + \frac{\partial \tau_y/\rho}{\partial z} \qquad (2)$$

in which τ_x and τ_y represent the horizontal turbulent stresses. The coordinate system is chosen such that the x axis is aligned with the geostrophic wind vector (with magnitude G). To explain the nocturnal IO B57 assumes that friction disappears at the onset of the NBL above the inversion layer and that friction remains zero during the night. Under this assumption, (1) and (2) become

$$\frac{\partial U}{\partial t} = fV \qquad (3)$$

and

$$\frac{\partial V}{\partial t} = f(G - U). \qquad (4)$$

This system can be solved by differentiating (3) and substituting (4). Assuming an initial profile at the onset
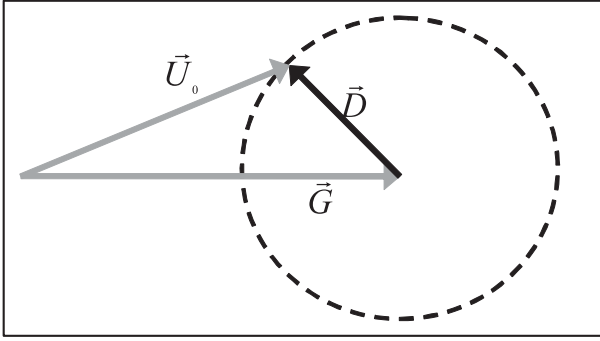
FIG. 1. At a certain height z, the deviation vector **D** rotates clockwise (NH) in time around the equilibrium vector (here **G**). The initial wind vector at z is denoted by U_0 (after B57).

of the inertial oscillation, $U = U_0$ and $V = V_0$ at $t = 0$, the solution reads

$$U - G = (V_0 - 0)\sin(ft) + (U_0 - G)\cos(ft) \quad (5)$$

and

$$V - 0 = (V_0 - 0)\cos(ft) - (U_0 - G)\sin(ft). \quad (6)$$

The reason for writing the solution in this unconventional form will become clear later, especially if we realize that the equilibrium solution of (3) and (4) is ($U_{eq} = G$, $V_{eq} = 0$) so that (5) and (6) represent undamped oscillations around this equilibrium. For each height, the amplitude of the oscillation equals the geostrophic departure D at sunset. This is illustrated by Figs. 1 and 2.

As stated in the introduction, B57 is applicable above the NBL where frictional effects can be assumed to be relatively small. An extension of the B57 theory is introduced below, which includes a parameterization of frictional effects within the NBL.

3. A model for the development of low-level jets due to inertial oscillations

As before, we start with the boundary layer equations (1) and (2):

$$\frac{\partial U}{\partial t} = fV + F_x(z, t) \quad (7)$$

and

$$\frac{\partial V}{\partial t} = f(G - U) + F_y(z, t), \quad (8)$$

where a shorthand notation is used for the kinematic turbulent stress divergences [$F_x(z, t) = \partial(\tau_x/\rho)/\partial z$ and $F_y(z, t) = \partial(\tau_y/\rho)/\partial z$]. For the system of equations a stationary (or equilibrium) solution is available through
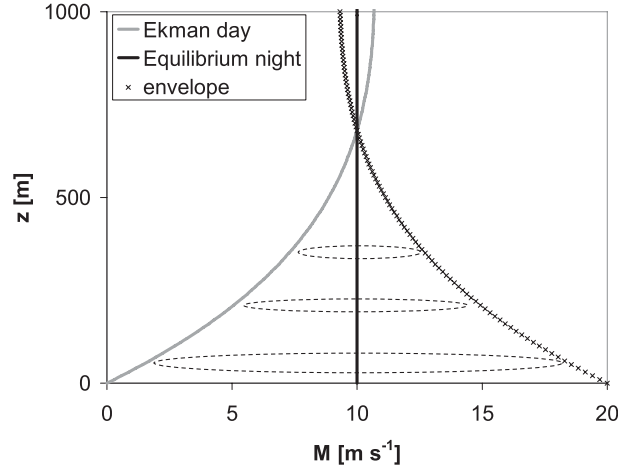

FIG. 2. Schematic illustration explaining IO around geostrophic equilibrium (after B57); M represents the wind speed (note that this way of presenting disregards directional effects; see section 6).

$$0 = fV_{eq} + F_{xeq}(z) \quad (9)$$

and

$$0 = f(G - U_{eq}) + F_{yeq}(z), \quad (10)$$

where U_{eq}, V_{eq} is the equilibrium solution. B57 simplified (7) and (8) by assuming the frictional terms to be zero. Rather than neglecting those terms, here we replace them by their equilibrium value obtained by (9) and (10). In other words: let us assume that the *actual friction* during and after evening transition *equals* the friction that would be present in the *equilibrium nocturnal boundary layer*; that is,

$$F_x(z, t) = F_{xeq}(z) \quad (11)$$

and

$$F_y(z, t) = F_{yeq}(z). \quad (12)$$

According to this assumption it is expected that most of the friction occurs over the depth of the NBL and that this friction is not very different from the frictional term in nocturnal equilibrium. Under this assumption, friction becomes a function of height only (and not of time). Although this is a rather crude approximation of reality, where vertical shear is time dependent, we want to investigate the extent to which the resulting set of equations captures key features of typical observed wind profiles. For more discussion on those issues, refer to section 7.

We apply assumptions (11) and (12) by inserting (9) and (10) into (7) and (8) and obtain

$$\frac{\partial(U - U_{eq})}{\partial t} = f(V - V_{eq}) \tag{13}$$

and

$$\frac{\partial(V - V_{eq})}{\partial t} = -f(U - U_{eq}). \tag{14}$$

For convenience, we have introduced U_{eq} and V_{eq} in the differential operator on the left-hand side (as $\partial U_{eq}/\partial t = \partial V_{eq}/\partial t = 0$) so that our equations are expressed in *departure from equilibrium* rather than in terms of geostrophic departure. Following the same procedure as before, the solution is

$$U - U_{eq} = (V_0 - V_{eq})\sin(ft) + (U_0 - U_{eq})\cos(ft) \tag{15}$$

and

$$V - V_{eq} = (V_0 - V_{eq})\cos(ft) - (U_0 - U_{eq})\sin(ft); \tag{16}$$

our main result. Here U_0 and U_{eq} represent the initial and equilibrium velocity components in the x direction (likewise for V_0 and V_{eq}). Equations (15) and (16) are general in the sense that they do not state anything about the specific closure assumptions used in order to find U_{eq} and V_{eq}. The B57 solutions [(5) and (6)] now become particular forms of (15) and (16) in the case: $U_{eq} = G$, $V_{eq} = 0$.

Two interesting characteristics of the solution appear. First, it occurs that at each height the IO is independent of the IO at other heights (a PDE is transformed into an ODE). Second, the oscillation itself is *undamped*. This seems a somewhat counterintuitive feature as "friction" is included in the analysis. Indeed, generally speaking, oscillations are damped by friction, but from our particular model friction is per definition *in phase* with the Coriolis terms. Note that, as a signature of BL friction, the flow within the NBL is cross-isobaric when averaged over a full oscillation period.

In the present study we assume that damping effects are nondominant during the course of the night, which is typically shorter than a full oscillation period. Although comparison with observational data (section 5) suggests that this assumption is not unrealistic, clearly more study on this aspect is required. In Fig. 3 the aforementioned aspects of (15) and (16) are illustrated. In this particular example the familiar Ekman (1905) solutions (next section) are chosen to represent both initial and equilibrium profiles.
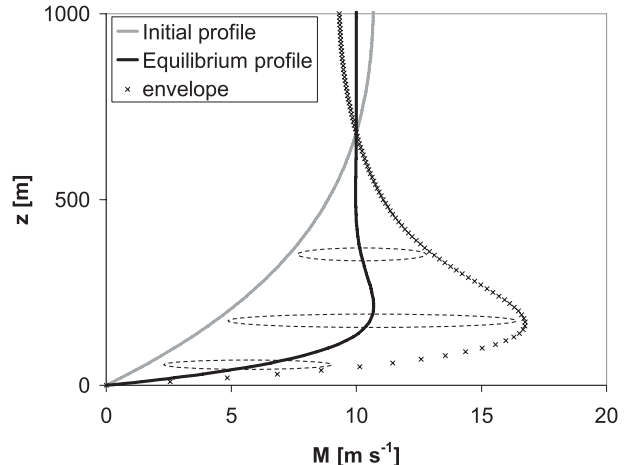

FIG. 3. As in Fig. 2 but with the nocturnal wind oscillating around the nocturnal equilibrium profile.

4. Illustrations

a. Low-level jet dynamics in an Ekman model

We illustrate the model by choosing Ekman solutions to represent the initial afternoon and the nocturnal equilibrium boundary layer. We choose this example because the Ekman concept is well known from an educational perspective. In Ekman terminology, the transition from day to night is represented by an abrupt change of the eddy diffusivity (Singh et al. 1993). In fact, in a recent paper, Shapiro and Fedorovich (2010) succeed in deriving exact analytical solutions for this specific case. Although their study is both very elegant and relevant from a theoretical point of view, their final result ends up rather complicated, which hampers the practical applicability aimed for in the present study.

In the Ekman model (see the appendix) turbulent stresses are parameterized by assuming constant eddy diffusivity, which yields the following solution:

$$U_{Ek} = G[1 - e^{-\gamma z}\cos(\gamma z)] \tag{17}$$

and

$$V_{Ek} = G[e^{-\gamma z}\sin(\gamma z)], \tag{18}$$

where $1/\gamma$ is the scale depth (m) of the boundary layer: $1/\gamma = \sqrt{2K/f}$, K the eddy diffusivity (m² s⁻¹), and f the Coriolis parameter (in the examples a value of 1.14×10^{-4} s⁻¹ is used to represent 52°N]. Let us consider the case where the ratio of scale depths of the afternoon to the nocturnal boundary layer is 5. We adopt $K_{afternoon} = 12.5$ and $K_{night} = 0.5$, corresponding to $\gamma_{night}/\gamma_{afternoon} \approx 500/100$.

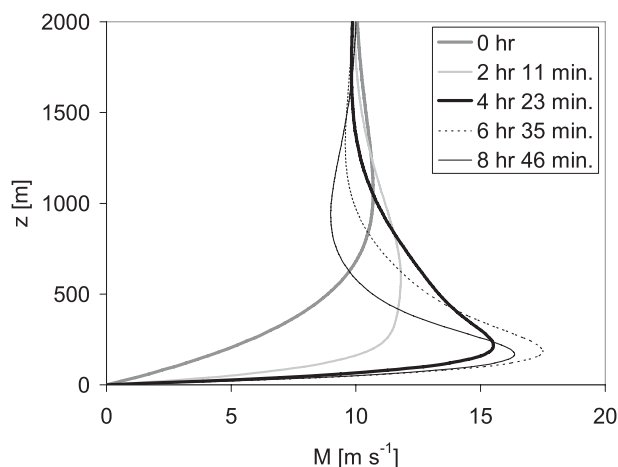FIG. 4. Low level jet dynamics predicted by (15) and (16), starting from an initial Ekman profile.

FIG. 5. Schematic picture of inertial oscillations using realistic initial wind profiles [gray line indicates a typical afternoon "radix profile" (Stull 1988)]. Both regions with forward and backward inertial observations are visible. Note that the "crossing point" has no absolute physical meaning in the sense that winds will oscillate at that level as well (owing to directional effects). Therefore, for a comprehensive picture a hodograph is used (section 6).

Next, we evaluate if the model predicts the occurrence of a LLJ: in (15) and (16) we insert $U_0 = U_{Ek}$, $V_0 = V_{Ek}$ using $K = 12.5$ and $U_{eq} = U_{Ek}$, $V_{eq} = V_{Ek}$ using $K = 0.5$. Figure 4 shows that, indeed, a LLJ is predicted. Initially the jet intensifies and sharpens while it descends during the night. Later the jet starts to weaken as the evolved time exceeds half the period of oscillation (8 h 46 min > π/f = 7 h 39 min). Those general features are also commonly observed in LLJs that originate from IOs (Van Ulden and Wieringa 1996). In principle, explicit time-dependent expressions for both jet height and magnitude can be derived by differentiating the expression for the magnitude of the wind vector with respect to height (not shown here). As shear effects usually minimize in the nose of the jet, predicting the nose height effectively implies prediction of the height $h(t)$ of the turbulent boundary layer.

b. From "Ekman" to realistic profiles

Although the illustration in the previous section suggests realistic jet dynamics, the applicability of Ekman profiles as an initial condition may be questioned. It is well known that as a result of efficient turbulent mixing, observed afternoon wind profiles are much more uniform (in magnitude and direction) than those described by typical Ekman profiles (Stull 1988).

Therefore, in Fig. 5 the dynamic consequences of realistic initial profiles are explored. First, it appears that at higher levels the afternoon departure from equilibrium is much more uniform than in the case of an Ekman initial profile (Fig. 3). From this, barotropic IOs are expected to be rather uniform with height. Interestingly, the initial profile crosses the equilibrium profile at some lower level. Since the model implies IOs of the initial profile around the equilibrium, this leads to a decrease
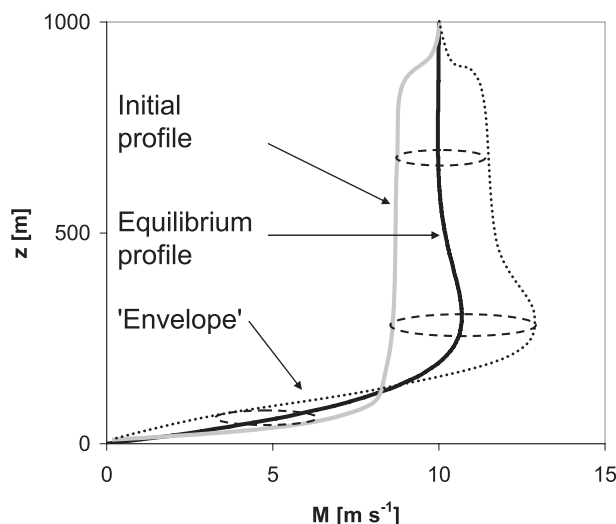
of wind speeds near the surface. In section 6 this aspect, referred to as backward inertial oscillations, is discussed. There we will show that Fig. 5 provides only limited information on IOs as it ignores the important *directional departure* from equilibrium. Alternatively, illustrations in the form of hodographs will be given.

Although afternoon BL profiles may be readily evaluated from observations, no such a priori information is available for the nocturnal equilibrium profile. As discussed in section 7, prediction of the equilibrium profile is nontrivial. Here, for reasons of simplicity, we assume an Ekman solution for the nocturnal equilibrium profile. We anticipate that nocturnal Ekman profiles are more realistic than afternoon Ekman profiles because in the NBL convective momentum transport is absent. Indeed, analytical work based on the Ekman concept (Zilitinkevich 1972; Nieuwstadt 1985) leads to reasonable BL height estimates and reasonable wind profiles as compared to observations. Although the Ekman approach is not unrealistic for the NBL as a whole, it clearly has its limitations close to the surface where the assumption of "constant eddy diffusivity" becomes unrealistic. Therefore, in section 7, we will point out viable paths for further improvement on this issue.

5. An observational example

In this section we will explore the practical applicability of the model by comparing it to observational data. We investigate a 7-night composite case constructed from
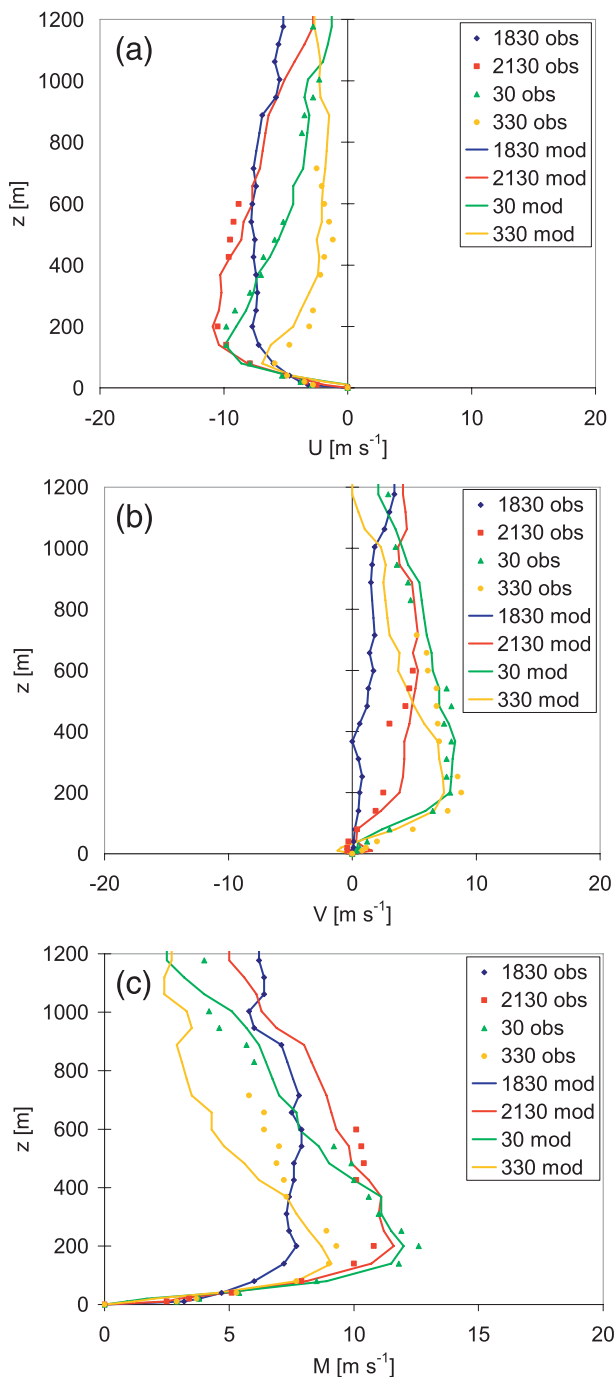
FIG. 6. Model results (lines) vs a composite of observational cases at Cabauw, velocity components presented by (a) U, (b) V, and (c) magnitude M.

wind observations at the KNMI Cabauw observatory in the Netherlands (Van Ulden and Wieringa 1996; Beljaars and Bosveld 1997). The comparison serves as an illustration and is not meant to explore the observations in full depth. For a more thorough analysis of those cases, as

well as for details on the observational methodology, we refer to Baas et al. (2009, 2010).

From a climatological study by Baas et al. (2010) it appears that at Cabauw most LLJs occur in fair-weather conditions with an easterly background flow. Those cases usually coincide with an anticyclone over Scandinavia and the synoptic weather pattern favors large-scale baroclinicity. This baroclinicity causes the geowind at Cabauw to decrease with height, which favors jet-shaped profiles. Fair-weather conditions are also favorable for nocturnal IOs, as the contrast in turbulence intensity between day and night is generally largest under those conditions. In addition to height variations of the geostrophic wind, systematic temporal variations of the geostrophic wind may also occur due to a diurnal cycle in the land–sea temperature contrast in the Netherlands (Van Delden 1993). However, in the present study we will ignore this latter effect, which is assumed to be of minor importance.

The fact that baroclinic situations are rule rather than exception in the Netherlands allows us to build a so-called *composite case*, following the methodology of Baas et al. (2010). The advantage of this approach is that random disturbances that occur on a case-to-case basis will average out, giving a clearer view of the IO itself. In turn, following the philosophy of Van de Wiel et al. (2003), Baas et al. classified NBLs according to their radiative and mechanical forcings: from an 8-yr database, eight "comparable" nights were selected with net radiation less than -30 W m^{-2} and a geostrophic wind ranging between 5 and 15 m s^{-1}. Furthermore, data around June were chosen in order to have comparable day lengths and predominantly southeasterly flows. The composite was formed by case averaging and is comparable to the one of Baas et al. (2010), except that two nights from 2008 were replaced by 19 and 20 August 2005 (for reasons of data availability).

The observations represent both mast data (up to 200 m) and observations from a wind profiler (Baas et al. 2010). From the profiler data the geostrophic wind $[U_g(z), V_g(z)]$ is prescribed according to $[U_g(z); V_g(z)] = [-7 + 6z/2000; 5 - 5z/2000]$. Equilibrium profiles may be found directly by inserting $[U_g(z), V_g(z)]$ in (A5) and (A6), where we adopt $1/\gamma \approx 80$ m, which gives a reasonable fit to the data. Since formally speaking (A5) and (A6) are only valid in the case of height-independent geostrophic wind, this is a pragmatic approximation that assumes the change in $\mathbf{G}(z)$ over the depth of the nocturnal boundary layer is relatively small (here typically $<10\%$). The initial profile is taken from the observations at 1830 UTC. The results are shown in Figs. 6a–c. The dynamic response of both the velocity components and their magnitude in the observations is captured
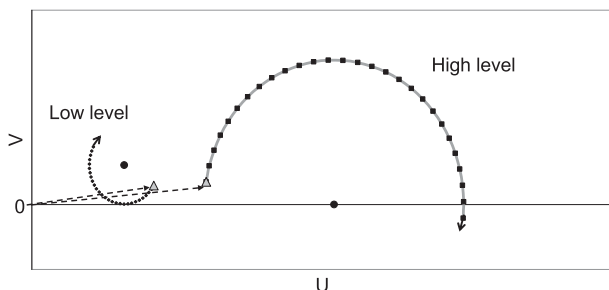
FIG. 7. Idealized hodographs showing typical low-level backward and high-level forward oscillations by inertial effects. Gray triangles indicate end points of the initial wind vectors (dashed); black dots refer to the (hypothetical) equilibrium vectors at both heights.
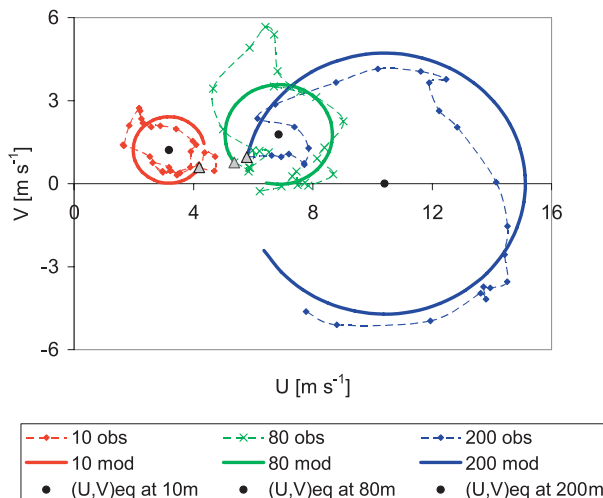

FIG. 8. Hodographs for three different levels observed at the Cabauw observatory on 15–16 Jul 2006. Observations are shown with thin dashed lines (each symbol represents a half-hour value); model results are shown with thick lines. Gray triangles indicate end point of the initial wind vectors; black dots correspond to the (supposed) equilibrium vectors (see text).

surprisingly well by the model. Although this comparison supports the practical potential of the model, it must be realized that more data analysis is necessary to draw more definite conclusions with regard to this aspect. In particular it would be interesting to extend the present analysis to other geographic areas with LLJs forced by inertial oscillations.

6. Decreasing evening winds due to backward inertial oscillations

In section 4 it was pointed out that realistic initial profiles imply a "crossing point" where the initial and equilibrium profile intersect. This will cause a backward inertial oscillation in the low-level wind below the crossing point, opposite to the more commonly known forward inertial oscillation, which manifests itself as the LLJ. Before we explore this further it is important to realize that Fig. 5 only shows the *magnitude* of the wind vector. Inertial oscillations, however, are also driven by *directional disequilibrium*. Somewhat counterintuitively, the crossing point itself will also be subject to IO! Formally speaking: as at some height $M_0(z_c) = M_{eq}(z_c)$, subscript c indicating crossing point, no height can be found where both $U_0 = U_{eq}$ and $V_0 = V_{eq}$ at the same height. This makes Fig. 5 somewhat misleading. Therefore, in the analysis below we will utilize hodographs to visualize directional effects.

In Fig. 7 two typical hodographs—for high and low levels—are sketched. The initial velocity vectors at both levels are indicated by dashed arrows (end points: gray triangles). As the initial situation refers to a well-mixed afternoon boundary layer, both magnitude and direction are relatively uniform as compared to the nighttime equilibrium vectors for those levels (indicated by the black dots). Because of IO both vectors turn clockwise around their equilibrium point (Northern Hemisphere). As we aligned our coordinate system along the upper-level equilibrium vector, the upper-level picture resembles the

B57 hodograph (Fig. 1), with an initially increasing wind vector magnitude. In contrast, clockwise rotation at the lower level implies an initial decrease of the magnitude of the wind vector. As such, the effect may contribute to the weakening of low-level winds in the early evening. Again, it is not that the magnitude of the initial vector is so much different from the equilibrium vector but mainly the difference in direction that causes the backward oscillation.

The concept in Fig. 7 is also found in observations. Figure 8 shows observed hodographs for three different levels for a case at the Cabauw observatory (15–16 July 2006). As before, we indicate initial velocity vectors by a gray triangle (1630 UTC). To compare the observations with (15) and (16), equilibrium wind vectors are needed. Previously, nocturnal equilibrium profiles were represented by Ekman profiles. Although this leads to satisfactory results for the jet as a whole, the method fails close to the ground where the assumption of constant diffusivity is clearly invalid. A better approach would consist of deriving equilibrium profiles by using more realistic K profiles. Such an approach is, however, nontrivial (see next section), and therefore we adopt a more practical method here. As the observed hodographs have a more or less circular shape, we are tempted to assume that the equilibrium vector is reasonably represented by the center of mass of the observations (indicated by black dots). Of course, this assumption, which ignores possible damping effects and assumes stationarity of external forcings, is rather crude,

but it may help for a qualitative understanding of the phenomena.

Figure 8 demonstrates that, apart from an initial disturbance, the evolution of the observed 200-m wind vector (blue) resembles a classical forward inertial oscillation. At the lowest level (red) the observations reveal a clockwise backward inertial oscillation (again apart from an initial disturbance). As such, the magnitude of the wind speed decreases initially in both model and observations (verified by looking at individual time stages). The midaltitude at 80 m (green) forms some kind of compromise between the extremes, as the orientation of the "opening" of the horseshoe hodograph changes with height. As in Fig. 7, the initial wind vectors (gray triangles) are much more unidirectional than the equilibrium vectors. We note that the hodographs of the 20-m and 140-m levels (not shown for clarity reasons) do fit into this picture, being a compromise between 10 and 40 m and between 80 and 200 m, respectively, so that IOs seem to change gradually with height.

The circular behavior of the low-level hodograph presented here is supported by the example from the Wangara experiment given by Thorpe and Guymer (1977). In their Fig. 6 the low-level hodograph describes a circular anticlockwise track (Southern Hemisphere) with initially decreasing wind speeds, similar to the clockwise example for the Northern Hemisphere presented here. By using an elegant two-layer bulk model Thorpe and Guymer were able to simulate some basic characteristics of forward inertial oscillations in the upper and backward inertial oscillations in the lower layer. However, their model seems to be overdamped in the lower layer as compared to the observations. As a result, the simulated hodograph does not follow the observed circular hodograph. Although their pioneering work facilitated the understanding of low-level wind dynamics [with successful applications in, e.g., Beyrich and Klose (1988, 1990), Andreas et al. (2000), and ReVelle and Nilsson (2008)], it presumed a distinct bulk character of the NBL with a "cut" at the inversion. In contrast, the present analysis supports a more continuous character of IO in the NBL, as judged from the gradual change in orientation of the opening of the hodographs.

It is important to note that even in this canonical example deviations from the idealistic picture are present in the initial stage of the oscillation. In general, all kind of physical effects may dominate over IOs in their influence on the wind profile, and hodographs will easily deviate from the idealistic picture above.

In heterogeneous circumstances, for example, differential horizontal momentum advection may strongly affect wind profiles, as shown in Beyrich and Klose (1987). But also in the homogeneous case, the afternoon transition period is notoriously complex and turbulent stresses generally suffer from significant nonstationarity (Mahrt 1981). This is also true during the night when bursts of turbulence may cause sudden vertical exchange of momentum. In fact, the inertial oscillations themselves are conducive to the occurrence of this bursting: as lower and upper levels show velocity tendencies in opposite directions, they will strive at some form of "velocity discontinuity." Consequently this will favor the occurrence of an inflection point. As an inflection point implies a maximum local (directional) shear, this implies a local minimum in the gradient Richardson number (Van Ulden and Wieringa 1996), favoring the generation of turbulence. In turn, the turbulence will be transported downward to drive so-called "top down" boundary layers (Mahrt and Vickers 2002; Ohya et al. 2008), and it will modify the shape of the hodographs. Finally, besides the Richardson number mechanism, the inflection point itself is known to be a potential cause of instability in nocturnal boundary layers (Newsome and Banta 2003; Sun et al. 2004; Mahrt 2008).

7. Discussion

a. Model assumption regarding constant turbulent stress

The key assumption in the new conceptual model lies in the fact that time-dependent turbulent friction $F(z, t)$ is parameterized by a constant frictional term: $F_{eq}(z)$. From the previous sections the advantage of such an approach has become clear. The model enables prediction of vertically continuous velocity profiles, in contrast to bulk models (Thorpe and Guymer 1977). The advantage over exact analytical models lies in the fact that the current model is simpler to apply and it does not rely on (often rather restricted) forms of turbulence closure so that actually observed data can be used as initial condition. Finally, the method provides a clear conceptual picture of inertial backward oscillations, consistent with previously known forward inertial oscillations.

Since, generally speaking, vertical shear is a function of both height and time, the solution presented here will inevitably deviate from reality. However, the close correspondence between the simplified solution and observational data suggests that the assumption of time independence has some validity. To assess generality, the analysis would benefit from comparison with other datasets, although it is realized that observational data are often subject to large-scale disturbances that cannot be captured by a model that assumes homogeneity (Baas et al. 2010). Such homogeneous comparison can be made with full analytical models (e.g., Shapiro and Fedorovich

2010) or with idealized simulations from numerical models (e.g., Svensson and Holtslag 2009) to improve on the assumptions within the current model.

b. The equilibrium state

Since Eqs. (15) and (16) predict IOs around the equilibrium vector, the success of the method partly depends on the ability to represent initial and equilibrium states. In contrast to the initial state, which may be available from observed profiles, the equilibrium profile has to be derived from some type of model by adopting a particular turbulence closure formulation. For general LLJ dynamics, previous results indicate that a simple Ekman model suffices. However, to predict more subtle effects such as backward inertial oscillations, more realistic equilibrium profiles are needed. Although it is not the purpose of the present work to elaborate on this issue, we will briefly discuss a viable route.

For a real predictive model, equilibrium profiles should be expressed in terms of *external forcing parameters* such as geostrophic wind and radiative forcing. Usually, equilibrium models of the NBL depart from a ''resistance law'' (Zilitinkevich and Esau 2005). In general, resistance laws model friction velocity as a function of geostrophic wind speed and local stability. By knowing the surface friction velocity, mean velocity profiles are found via similarity relations (Blackadar and Tennekes 1968). Finally, velocity profiles take the typical form: $U(z)$, $V(z) = f(G, f, z_0, L)$, with L the Obukhov length scale (Zilitinkevich 1975; Nieuwstadt 1981).

Apart from information on local stability needed via L, this expression uses external geostrophic forcing. For true prediction, L is to be expressed in terms of external parameters as well. In principle, this can only be achieved by incorporating the full thermodynamic equation for temperature with a surface energy balance as a lower boundary condition. However, from a detailed observational study Holtslag and de Bruin (1988) showed that the surface energy balance may be simplified into a semiempirical expression for the temperature scale θ_*: $\theta_* = f(u_*, Q_i)$, which in our case implies $L = f(u_*, Q_i)$. Here Q_i is the so-called ''isothermal'' net radiation that is based on external longwave radiative parameters like the clear-air emissivity and cloud cover. As such, this leads to a closed system in terms of external parameters so that, at least in principle, the methodology could be extended to have predictive potential. However, it is realized that this step is far from trivial at this point.

8. Summary and conclusions

In the present work the B57 concept for nocturnal IO is extended. Rather than assuming that frictional effects fully disappear at the onset of the nocturnal boundary layer, frictional effects within the NBL are parameterized by assuming that friction is equal to the friction in the nighttime equilibrium solution. As a result, the nocturnal velocity profile does not describe an inertial oscillation around the geostrophic wind vector, but rather around the equilibrium wind vector. From this new solution, inertial low-level jet dynamics can be predicted. Preliminary analysis shows that the model performs well in comparison with observations when a simple Ekman model is used to represent the equilibrium state in combination with a realistic initial velocity profile.

In addition to jet dynamics, the model suggests the existence of so-called backward inertial oscillations. Those oscillations appear also to be present in observations. We suggest that this backward inertial oscillation forms an important mechanism behind the weakening of low-level winds during the afternoon transition. Both observational and theoretical modeling studies are needed to explore this phenomenon further and to assess the validity of the underlying assumptions.

APPENDIX

Ekman Solutions

Following Ekman (1905), turbulent stresses are parameterized by assuming constant eddy diffusivity K. The boundary layer equations (1) and (2) become

$$\frac{\partial U}{\partial t} = fV + K\frac{\partial^2 U}{\partial z^2} \tag{A1}$$

and

$$\frac{\partial V}{\partial t} = f(G - U) + K\frac{\partial^2 V}{\partial z^2}. \tag{A2}$$

For the stationary case (A1) and (A2) lead to the well-known Ekman solutions (e.g., Stull 1988; Fig. A1):
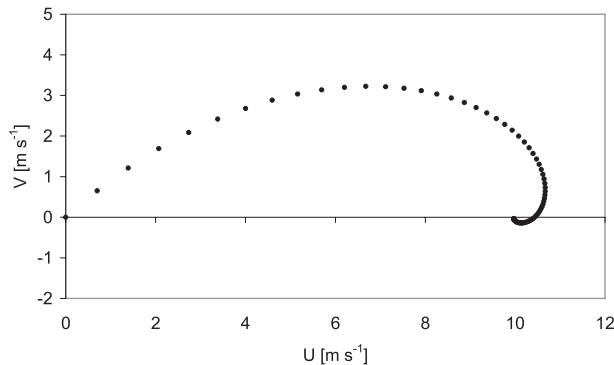
$$U_{Ek} = G[1 - e^{-\gamma z}\cos(\gamma z)] \tag{A3}$$

and

FIG. A1. An example of an Ekman spiral with $G = 10$ m s^{-1} and $f = 1.14 \times 10^{-4}$ s^{-1}. Each dot corresponds to a different height (here arbitrary values depending on the particular choice of K).

$$V_{Ek} = G[e^{-\gamma z} \sin(\gamma z)], \quad (A4)$$

where $\gamma = \sqrt{f/(2K)}$ (m^{-1}). In the above the coordinate system is chosen such that the x axis is aligned with the direction of the geostrophic wind. Computing the Ekman spiral, as in Fig. A1, in the first mathematical quadrant facilitates physical understanding. In practical applications, where the geowind is given in a fixed coordinate system, the Ekman solutions (A3) and (A4) have to be replaced by

$$U = U_g - U_g e^{-\gamma z} \cos(\gamma z) - V_g e^{-\gamma z} \sin(\gamma z) \quad (A5)$$

and

$$V = V_g - V_g e^{-\gamma z} \cos(\gamma z) + U_g e^{-\gamma z} \sin(\gamma z). \quad (A6)$$

Again, (15) and (16) hold for this case.

REFERENCES

Andreas, E. L., K. J. Claffey, and A. P. Makshtas, 2000: Low-level atmospheric jets and inversions over the western Weddell Sea. *Bound.-Layer Meteor.,* **97,** 459–486.

Baas, P., F. C. Bosveld, H. Klein Baltink, and A. A. M. Holtslag, 2009: A climatology of nocturnal low-level jets at Cabauw. *J. Appl. Meteor. Climatol.,* **48,** 1627–1642.

——, ——, G. Lenderink, E. Meijgaard, and A. A. M. Holtslag, 2010: How to design single-column model experiments for comparison with observed nocturnal low-level jets at Cabauw? *Quart. J. Roy. Meteor. Soc.,* **136,** 671–689, doi:10.1002/qj.592.

Banta, R. M., 2008: Stable boundary-layer regimes from the perspective of the low-level jet. *Acta Geophys.,* **56,** 58–87.

——, R. K. Newsom, J. K. Lundquist, Y. L. Pichugina, R. L. Coulter, and L. Mahrt, 2002: Nocturnal low-level jet characteristics over Kansas during CASES-99. *Bound.-Layer Meteor.,* **105,** 221–252.

——, Y. L. Pichugina, and R. K. Newsom, 2003: Relationship between the low-level jet properties and turbulence kinetic energy in the nocturnal stable boundary layer. *J. Atmos. Sci.,* **60,** 2549–2555.

——, ——, and W. A. Brewer, 2006: Turbulent velocity variance profiles in the stable boundary layer generated by a nocturnal low-level jet. *J. Atmos. Sci.,* **63,** 2700–2719.

Beljaars, A. C. M., and F. C. Bosveld, 1997: Cabauw data for the validation of land surface parameterizations. *J. Climate,* **10,** 1172–1193.

Beyrich, F., 1994: Sodar observations of the stable boundary layer height in relation to the nocturnal low-level jet. *Meteor. Z.,* **3,** 29–34.

——, and B. Klose, 1987: Modellierung nächtlicher niedertroposphärischer Windmaxima. I: Theoretische Betrachtungen. *Z. Meteor.,* **37,** 333–347.

——, and ——, 1988: Some aspects of modelling low-level jets. *Bound.-Layer Meteor.,* **43,** 1–14.

——, and ——, 1990: Modellierung nächtlicher niedertroposphärischer Windmaxima. II: Modellverifikation. *Z. Meteor.,* **40,** 30–37.

Blackadar, A. K., 1957: Boundary layer wind maxima and their significance for the growth of nocturnal inversions. *Bull. Amer. Meteor. Soc.,* **38,** 283–290.

——, and H. Tennekes, 1968: Asymptotic similarity in neutral barotropic planetary boundary layers. *J. Atmos. Sci.,* **25,** 1015–1020.

Ekman, V. W., 1905: On the influence of the Earth's rotation on ocean currents. *Arkiv. Matematik. Astron. Fysik.,* **2,** 1–53.

Holtslag, A. A. M., and H. A. R. de Bruin, 1988: Applied modelling of the nighttime surface energy balance over land. *Bound.-Layer Meteor.,* **27,** 689–704.

Liechti, F., and E. Schaller, 1999: The use of low-level jets by migrating birds. *Naturwissenschaften,* **86,** 549–551.

Lundquist, J. K., 2003: Intermittent and elliptical inertial oscillations in the atmospheric boundary layer. *J. Atmos. Sci.,* **60,** 2661–2673.

Mahrt, L., 1981: The early evening boundary layer transition. *Quart. J. Roy. Meteor. Soc.,* **107,** 329–343.

——, 1998: Stratified atmospheric boundary layers and breakdown of models. *Theor. Comput. Fluid Dyn.,* **11,** 263–279.

——, 2008: The influence of transient flow distortion on turbulence in stable weak-wind conditions. *Bound.-Layer Meteor.,* **127,** 1–16.

——, and D. Vickers, 2002: Contrasting vertical structures of nocturnal boundary layers. *Bound.-Layer Meteor.,* **105,** 351–363.

McNider, R. T., M. D. Moran, and R. A. Pielke, 1988: Influence of diurnal and inertial boundary-layer oscillations on long range dispersion. *Atmos. Environ.,* **22,** 2445–2462.

Newsome, R. K., and R. W. Banta, 2003: Shear-flow instability in the stable boundary layer as observed by Doppler lidar during CASES-99. *J. Atmos. Sci.,* **60,** 16–33.

Nieuwstadt, F. T. M., 1981: The steady-state height and resistance laws of the nocturnal boundary layer: Theory compared with Cabauw observations. *Bound.-Layer Meteor.,* **20,** 3–17.

——, 1985: A model for the stationary, stable boundary layer. *Turbulence and Diffusion in Stable Environments,* J. C. R. Hunt, Ed., Clarendon, 149–179.

Ohya, Y., R. Nakamura, and T. Uchida, 2008: Intermittent bursting of turbulence in a stable boundary layer with low-level jet. *Bound.-Layer Meteor.,* **126,** 349–363.

Ostdiek, V., and W. Blumen, 1997: A dynamic trio: Inertial oscillation, deformation frontogenesis, and the Ekman–Taylor boundary layer. *J. Atmos. Sci.,* **54,** 1490–1502.

ReVelle, D. O., and E. D. Nilsson, 2008: Summertime low-level jets, over the high-latitude Arctic Ocean. *J. Appl. Meteor. Climatol.,* **47,** 1770–1784.

Shapiro, A., and E. Fedorovich, 2009: Nocturnal low-level jet over a shallow slope. *Acta Geophys.,* **57,** 950–980.

——, and ——, 2010: Analytical description of a nocturnal low-level jet. *Quart. J. Roy. Meteor. Soc.,* **136,** 1255–1262.

Singh, M. P., R. T. McNider, and J. T. Lin, 1993: An analytical study of diurnal wind-structure variations in the boundary layer and the low-level nocturnal jet. *Bound.-Layer Meteor.,* **63,** 397–423.

Storm, B., J. Dudhia, S. Basu, A. Swift, and I. Giammanco, 2009: Evaluation of the Weather Research and Forecasting model on forecasting low-level jets: Implication for wind energy. *Wind Energy,* **12,** 81–90.

Stull, R. B., 1988: *An Introduction to Boundary Layer Meteorology.* Kluwer, 670 pp.

Sun, J., and Coauthors, 2004: Atmospheric disturbances that generate intermittent turbulence in nocturnal boundary layers. *Bound.-Layer Meteor.,* **110,** 255–279.

Svensson, G., and A. A. M. Holtslag, 2009: Analysis of model results for the turning of the winds and the related momentum fluxes in the stable boundary layer. *Bound.-Layer Meteor.,* **132,** 261–277.

Tan, Z.-M., and M. M. Farahani, 1998: An analytical study of the diurnal variations of wind in a semi-geostrophic Ekman boundary layer model. *Bound.-Layer Meteor.,* **86,** 313–332.

Thorpe, A. J., and T. H. Guymer, 1977: The nocturnal jet. *Quart. J. Roy. Meteor. Soc.,* **103,** 633–653.

Van Delden, A. J., 1993: Observational evidence of the wave-like character of the sea breeze effect. *Beitr. Phys. Atmos.,* **66,** 63–72.

Van de Wiel, B. J. H., A. F. Moene, O. K. Hartogensis, H. A. R. De Bruin, and A. A. M. Holtslag, 2003: Intermittent turbulence in the stable boundary layer over land. Part III: A classification for observations during CASES-99. *J. Atmos. Sci.,* **60,** 2509–2522.

Van Ulden, A. P., and J. Wieringa, 1996: Atmospheric boundary layer research at Cabauw. *Bound.-Layer Meteor.,* **78,** 39–69.

Weil, J. C., E. G. Patton, and P. P. Sullivan, 2006: Lagrangian modeling of dispersion in the stable boundary layer. Extended Abstracts, *17th Symp. on Boundary Layers and Turbulence,* San Diego, CA, Amer. Meteor. Soc., J3.4. [Available online at http://ams.confex.com/ams/pdfpapers/111205.pdf.]

Whiteman, D. C., X. Bian, and S. Zhong, 1997: Low-level jet climatology from enhanced rawinsonde observations at a site in the Southern Great Plains. *J. Appl. Meteor.,* **36,** 1363–1376.

Wittich, K. P., J. Hartmann, and R. Roth, 1986: On nocturnal wind shear with a view to engineering applications. *Bound.-Layer Meteor.,* **37,** 215–227.

Zilitinkevich, S. S., 1972: On the determination of the height of the Ekman boundary layer. *Bound.-Layer Meteor.,* **3,** 141–145.

——, 1975: Resistance laws and prediction equations for the depth of the planetary boundary layer. *J. Atmos. Sci.,* **32,** 741–752.

——, and I. N. Esau, 2005: Resistance and heat-transfer laws for stable and neutral planetary boundary layers: Old theory advanced and re-evaluated. *Quart. J. Roy. Meteor. Soc.,* **131,** 1863–1892.